Appendix A FaBCoM TeSt Experimental Modal Analysis Results

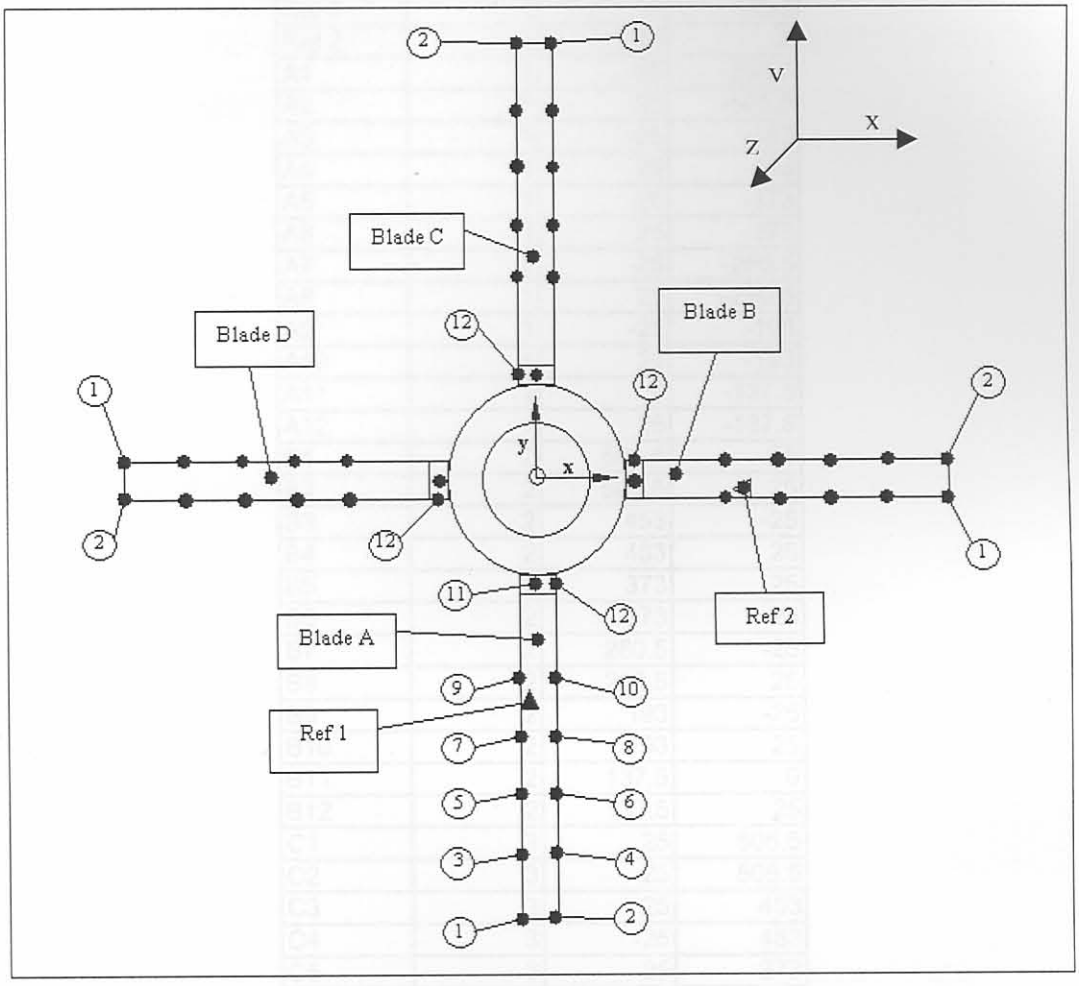

Figure A-1: Experimental Modal Analysis Measurement Point Locations

Table A-1: Experimental Modal Analyses Measurement Point Locations

Point #	Blade #	X	Y
		[mm]	[mm]
Ref 1	1	-8	-223
Ref 2	2	223	-8
A1	1	-25	-505.5
A2	1	25	-505.5
A3	1	-25	-453
A4	1	25	-453
A5	1	-25	-373
A6	1	25	-373
A7	1	-25	-280.5
A8	1	25	-280.5
A9	1	-25	-193
A10	1	25	-193
A11	1	0	-137.5
A12	1	25	-137.5
B1	2	505.5	-25
B2	2	505.5	25
B3	2	453	-25
B4	2	453	25
B5	2	373	-25
B6	2	373	25
B7	2	280.5	-25
B8	2	280.5	25
B9	2	193	-25
B10	2	193	25
B11	2	137.5	0
B12	2	137.5	25
C1	3	25	505.5
C2	3	-25	505.5
C3	3	25	453
C4	3	-25	453
C5	3	25	373
C6	3	-25	373
C7	3	25	280.5
C8	3	-25	280.5
C9	3	25	193
C10	3	-25	193
C11	3	0	137.5
C12	3	-25	137.5
D1	4	-505.5	25
D2	4	-505.5	-25
D3	4	-453	25
D4	4	-453	-25
D5	4	-373	25
D6	4	-373	-25
D7	4	-280.5	25
D8	4	-280.5	-25
D9	4	-193	25
D10	4	-193	-25

Table A-2 graphically compares experimental and numerical mode shapes with significant MAC. The MAC values between the mode shapes are given along with their mode shape numbers and frequencies.

Table A-2: Graphical Experimental and Numerical Mode Shape Comparison

Experimental	Numerical
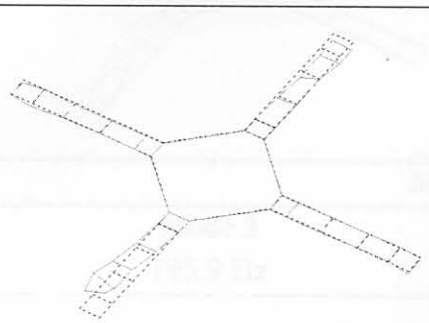	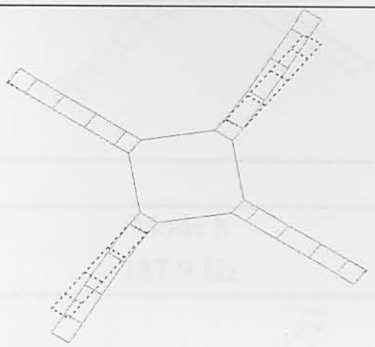
MAC = 0.78	
Mode 1 30.7 Hz	Mode 3 30.9 Hz
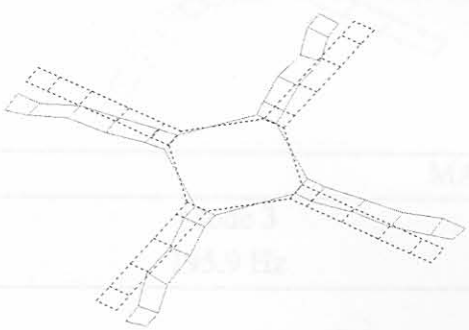	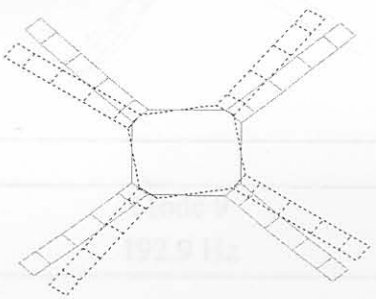
MAC = 0.93	
Mode 2 57.2 Hz	Mode 5 68.3 Hz
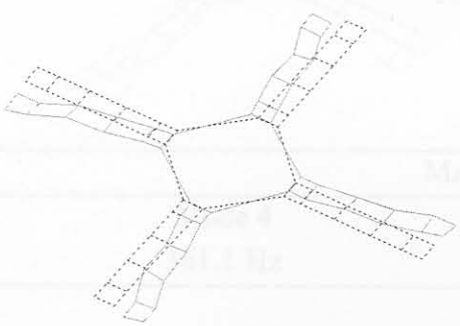	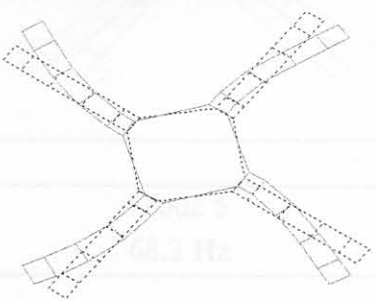
MAC = 0.58	
Mode 2 57.2 Hz	Mode 19 417 Hz

Experimental	Numerical
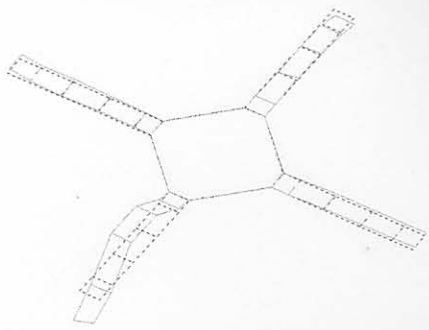	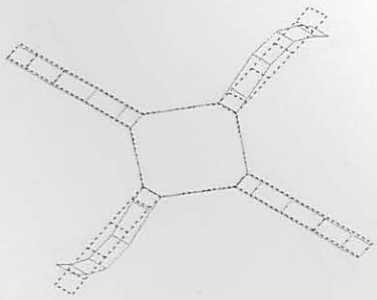
MAC = 0.37	
Mode 3 195.9 Hz	Mode 8 187.9 Hz
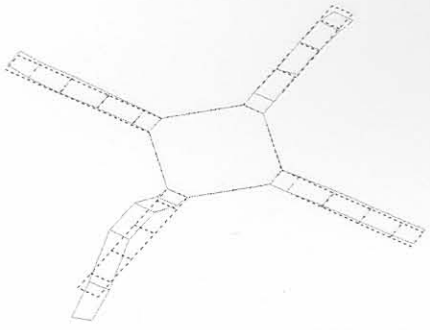	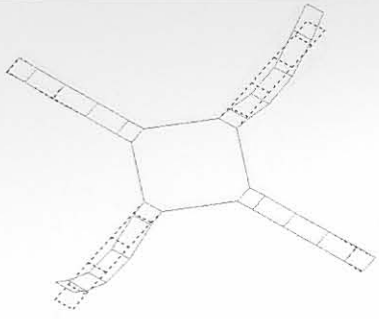
MAC = 0.62	
Mode 3 195.9 Hz	Mode 9 192.9 Hz
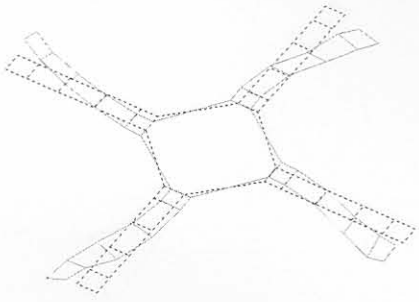	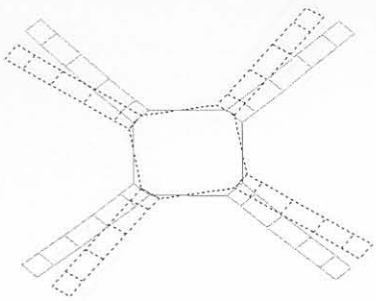
MAC = 0.52	
Mode 4 361.1 Hz	Mode 5 68.3 Hz

Experimental	Numerical
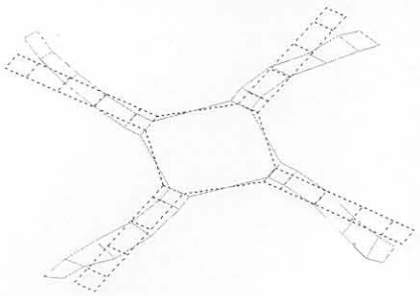	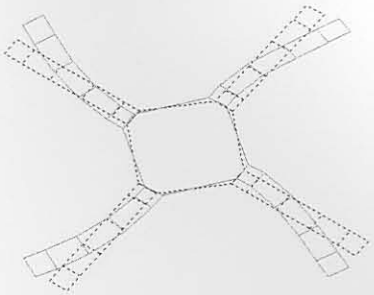
MAC = 0.80	
Mode 4 361.1 Hz	Mode 19 417 Hz
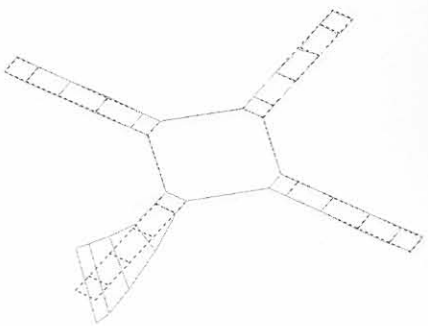	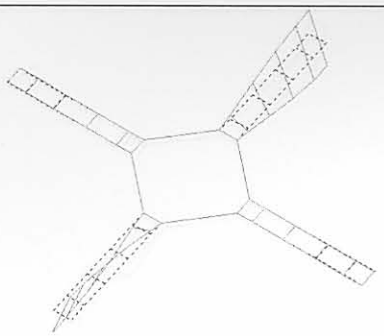
MAC = 0.47	
Mode 5 422 Hz	Mode 17 404.8 Hz
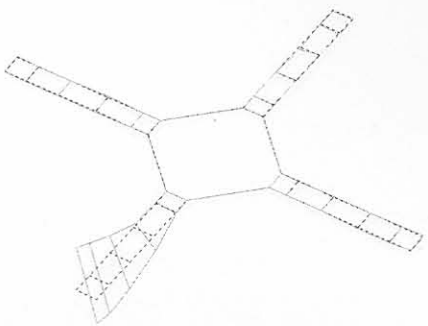	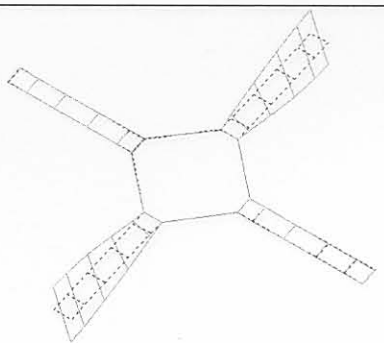
MAC = 0.44	
Mode 5 422 Hz	Mode 18 405 Hz

Experimental	Numerical
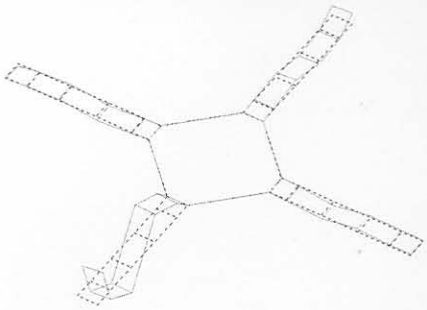	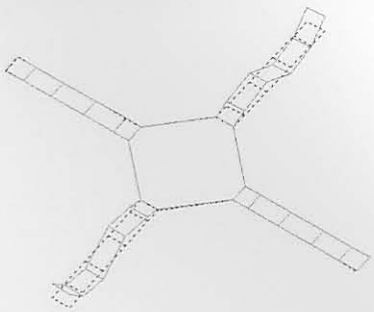
MAC = 0.70	
Mode 6 542 Hz	Mode 22 538 Hz
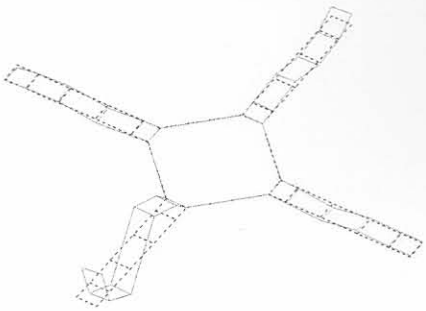	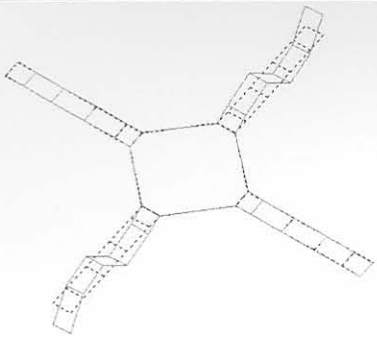
MAC = 0. 31	
Mode 6 542 Hz	Mode 23 541.3 Hz
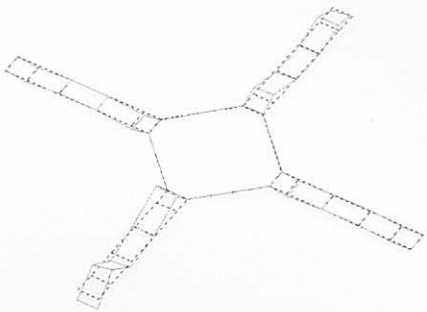	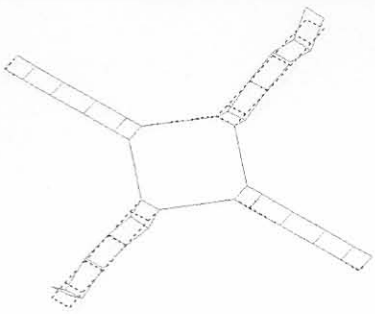
MAC = 0.60	
Mode 7 1058.9 Hz	Mode 26 1049.3 Hz

Experimental	Numerical
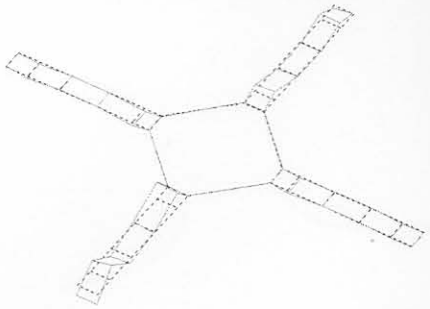	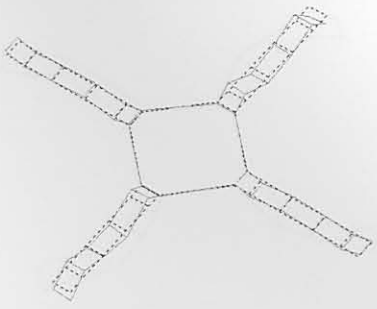
MAC = 0.50	
Mode 7 1058.9 Hz	Mode 51 2630.6 Hz
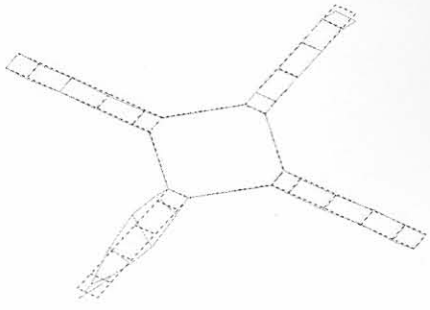	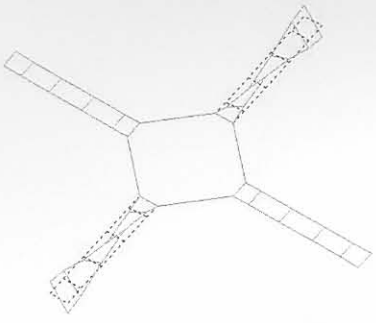
MAC = 0.33	
Mode 8 1278.1 Hz	Mode 30 1220 Hz
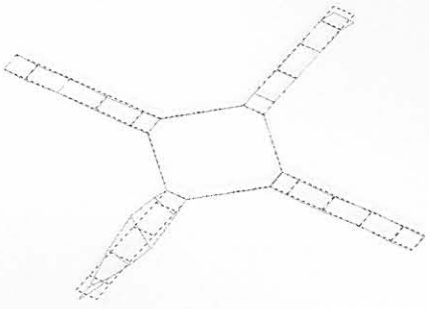	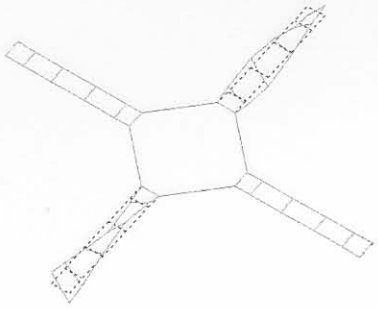
MAC = 0.43	
Mode 8 1278.1 Hz	Mode 31 1220 Hz

Experimental	**Numerical**
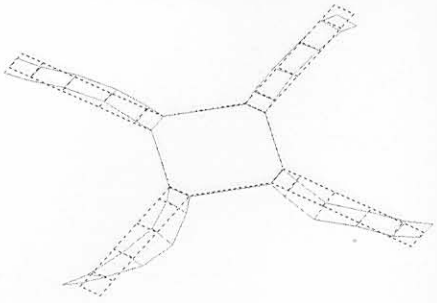	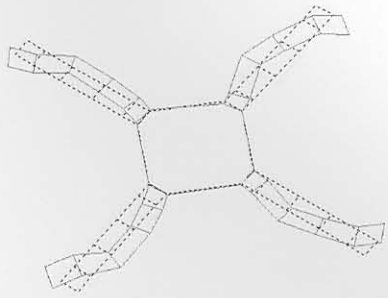
MAC = 0.48	
Mode 9 1390.3 Hz	Mode 33 1623.2 Hz
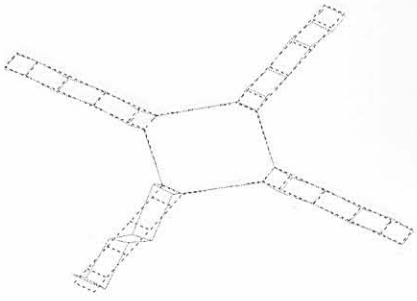	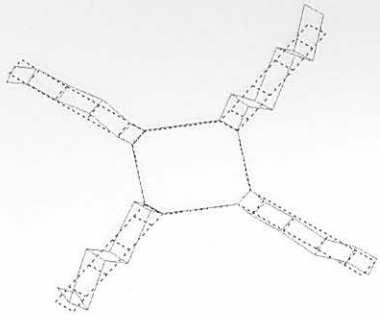
MAC = 0.41	
Mode 10 1648.9 Hz	Mode 38 1715.8 Hz
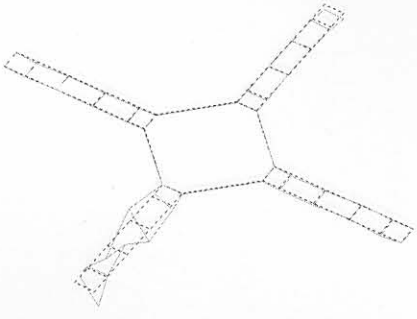	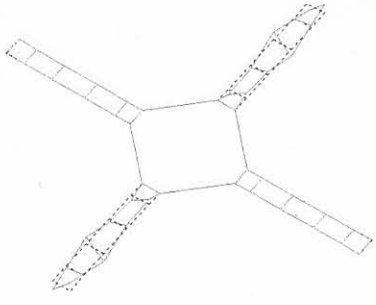
MAC = 0.35	
Mode 12 2490.9 Hz	Mode 46 2061.4 Hz

Experimental	Numerical
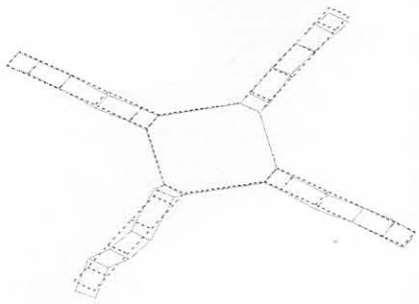	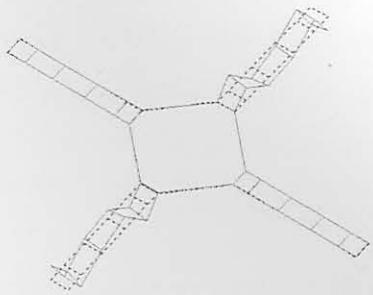
MAC = 0.34	
Mode 13 2820.1 Hz	Mode 50 2585.2 Hz
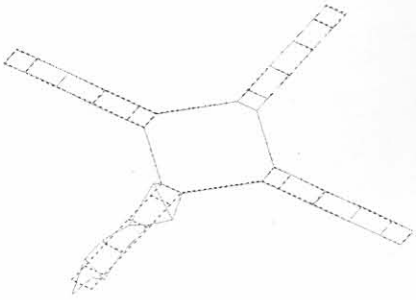	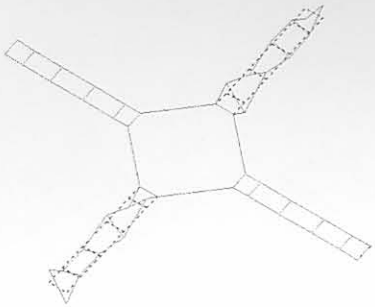
MAC = 0.44	
Mode 14 3282.1 Hz	Mode 54 2943.6 Hz
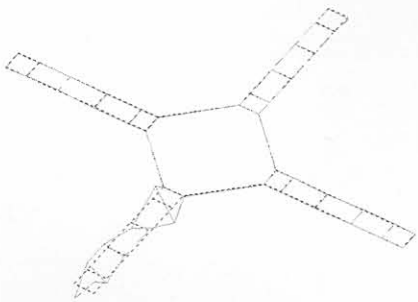	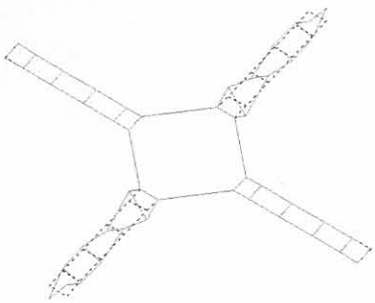
MAC = 0.38	
Mode 14 3282.1 Hz	Mode 55 2943.9 Hz

Experimental	Numerical
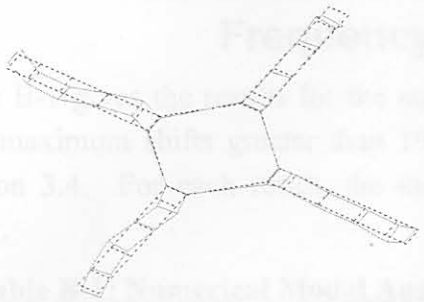	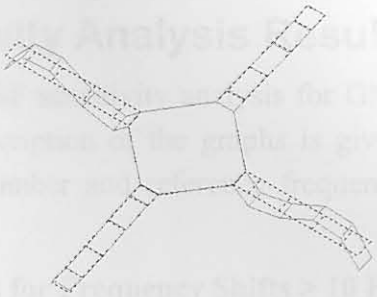
MAC = 0.37	
Mode 16 3733.1 Hz	Mode 59 3487.8 Hz

Appendix B Numerical Global Mode Shape Frequency Sensitivity Analysis Results

Table B-1 gives the results for the numerical GMSF sensitivity analysis for GMSFs with maximum shifts greater than 10 Hz. A description of the graphs is given in Section 3.4. For each result, the mode shape number and reference frequency is given.

Table B-1: Numerical Modal Analysis Results for Frequency Shifts > 10 Hz

<table>
<tr><td> 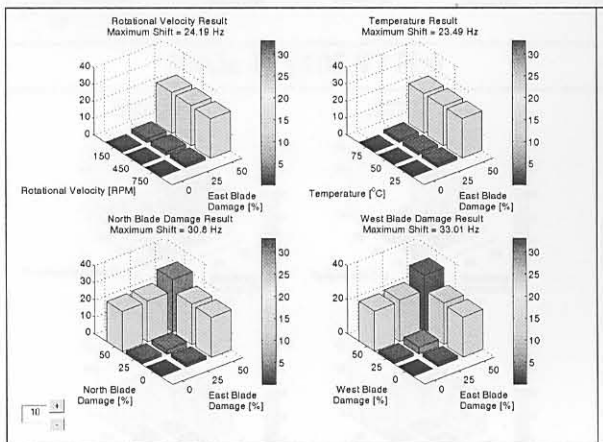
</td><td> 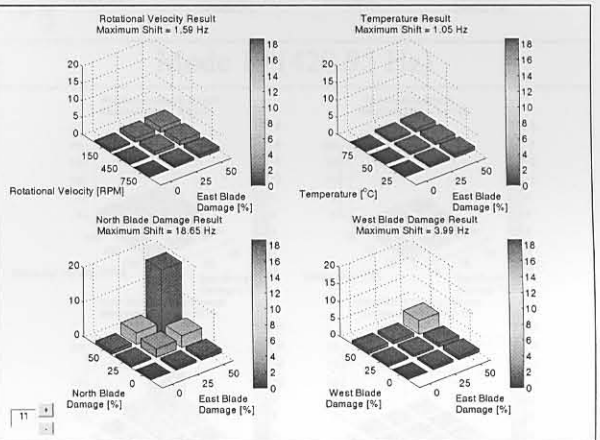
</td></tr>
<tr><td>Mode 10 (241.2 Hz)</td><td>Mode 11 (242.24 Hz)</td></tr>
<tr><td> 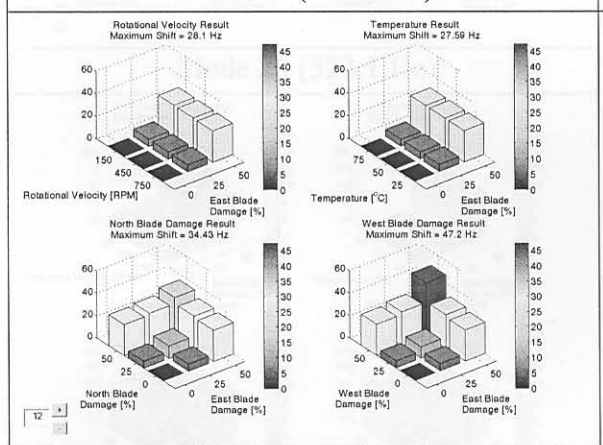
</td><td> 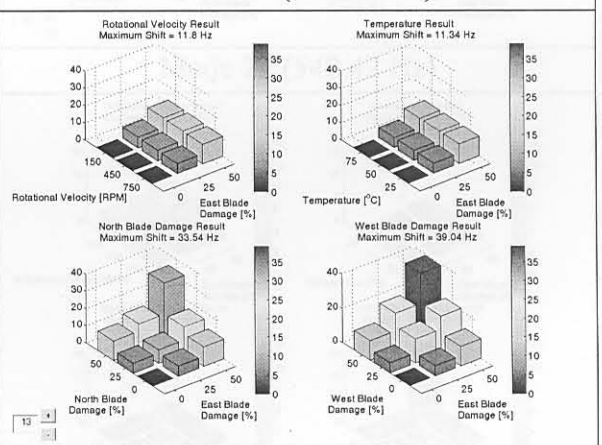
</td></tr>
<tr><td>Mode 12 (288.13 Hz)</td><td>Mode 13 (310.49 Hz)</td></tr>
<tr><td> 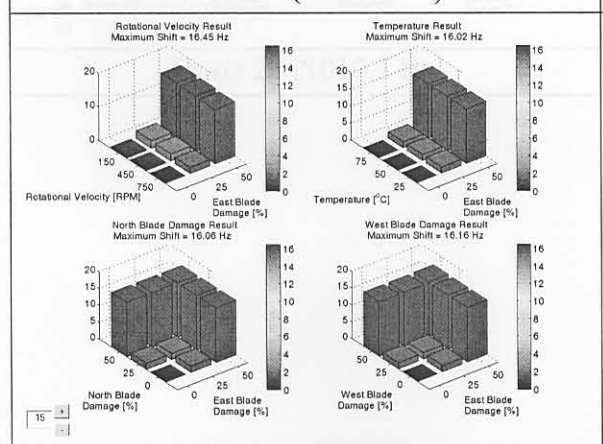
</td><td> 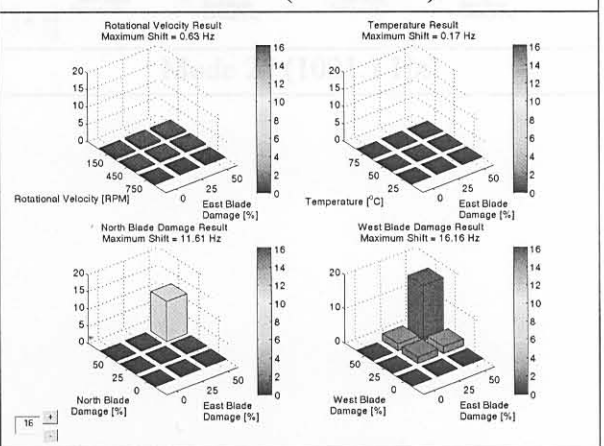
</td></tr>
<tr><td>Mode 15 (399.08 Hz)</td><td>Mode 16 (399.53 Hz)</td></tr>
</table>

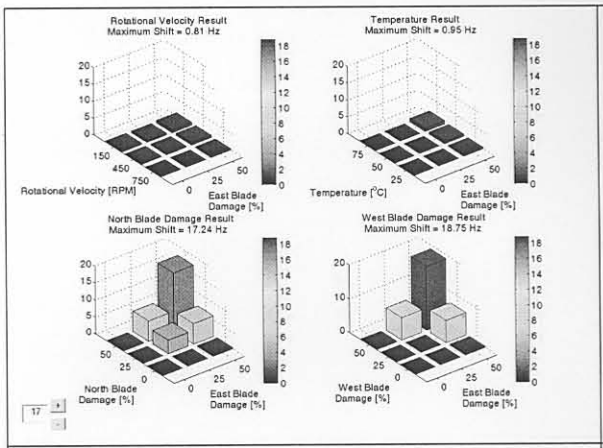

Mode 17 (405.97 Hz)

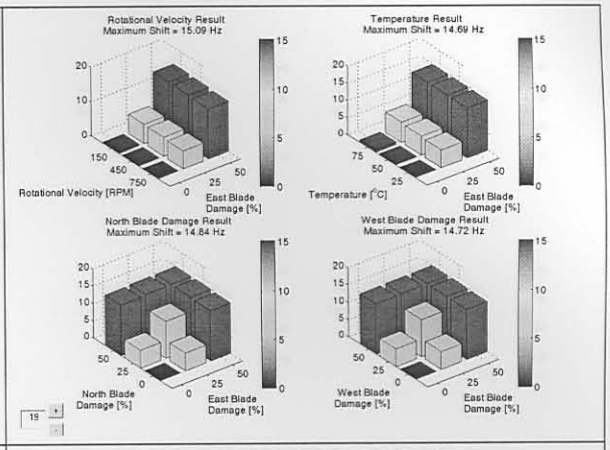

Mode 19 (420.95 Hz)

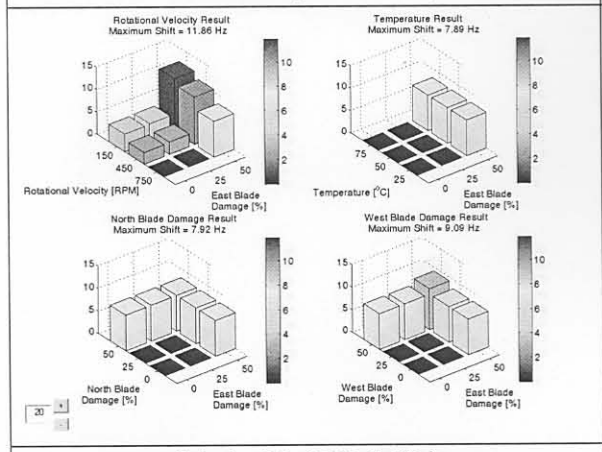

Mode 20 (523.1 Hz)

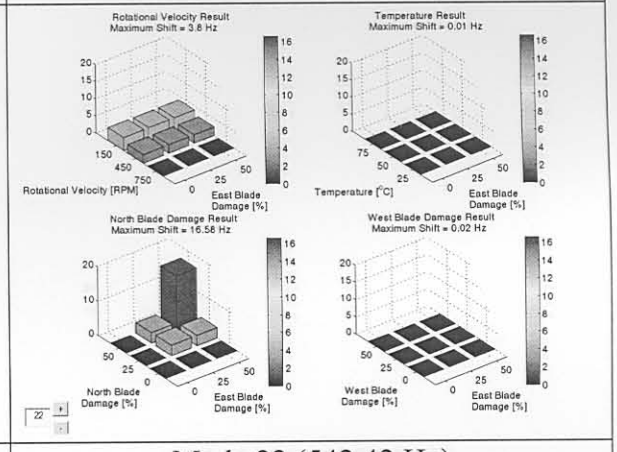

Mode 22 (542.42 Hz)

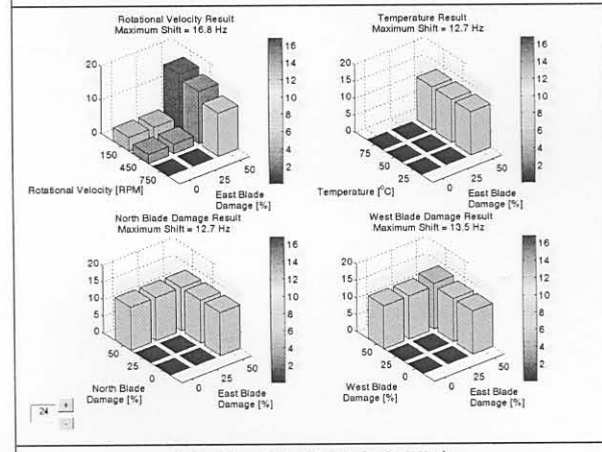

Mode 24 (1019.3 Hz)

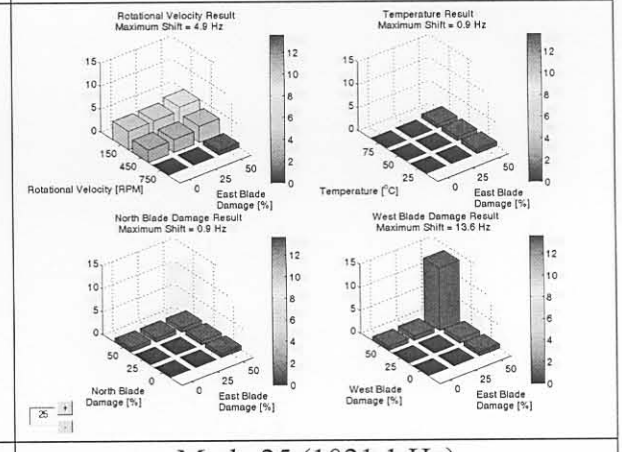

Mode 25 (1021.1 Hz)

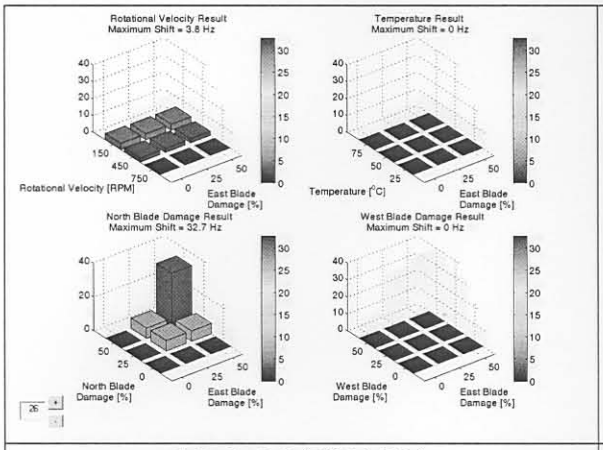

Mode 26 (1054 Hz)

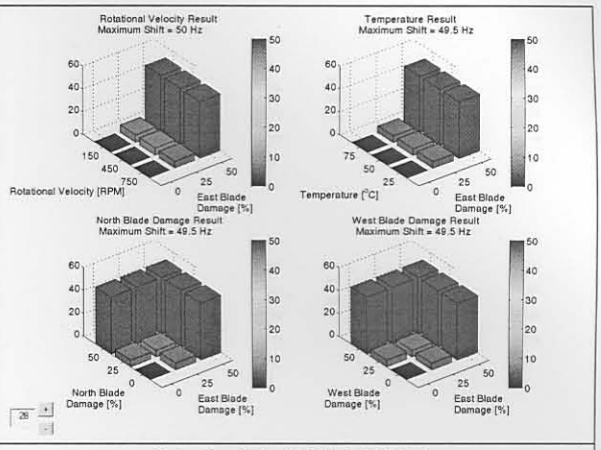

Mode 28 (1201.7 Hz)

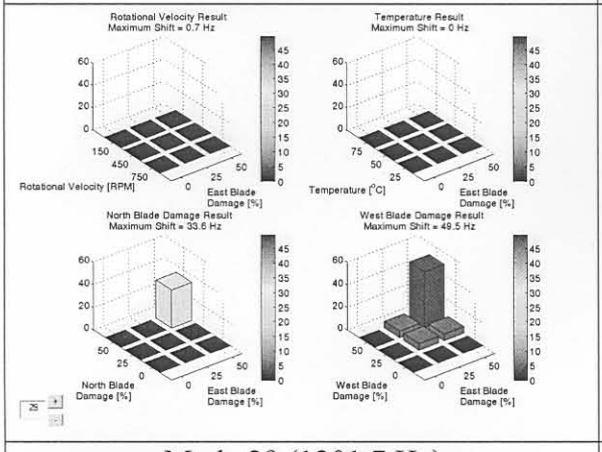

Mode 29 (1201.7 Hz)

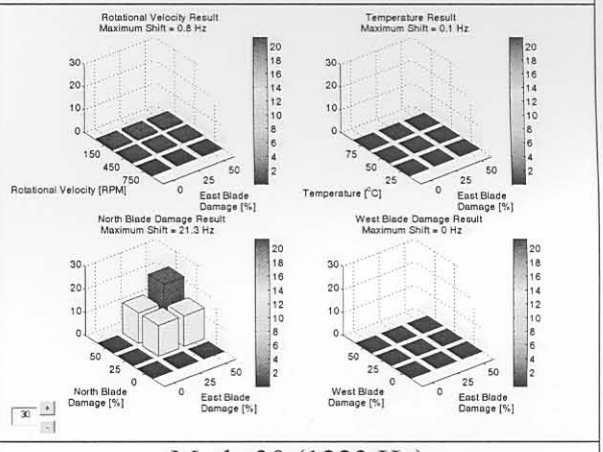

Mode 30 (1223 Hz)

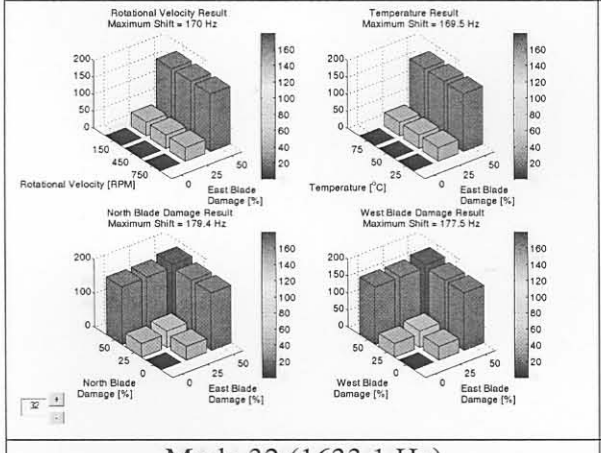

Mode 32 (1633.1 Hz)

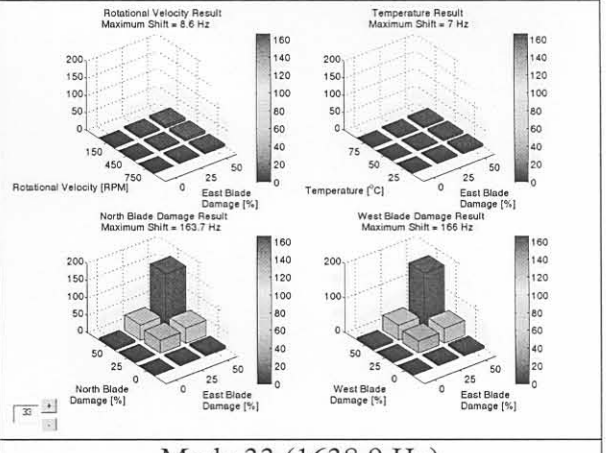

Mode 33 (1638.9 Hz)

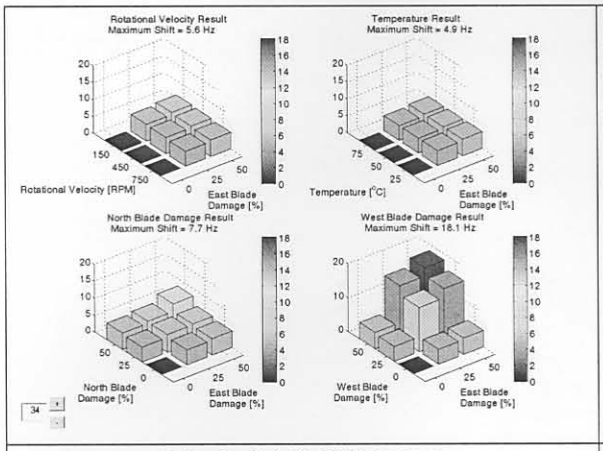

Mode 34 (1648.3 Hz)

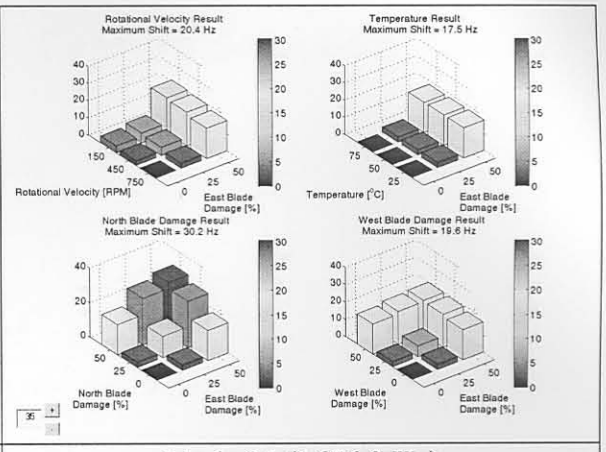

Mode 35 (1676.3 Hz)

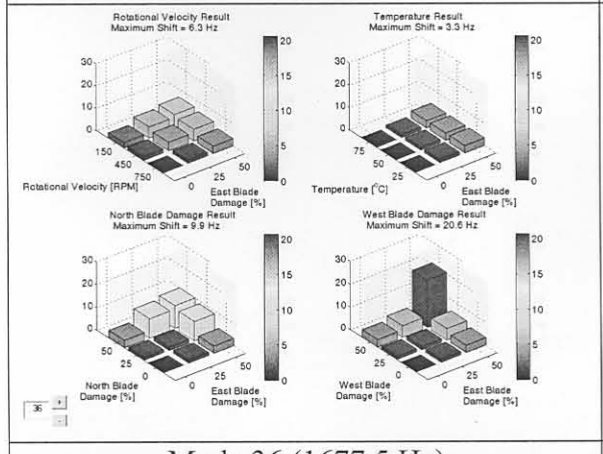

Mode 36 (1677.5 Hz)

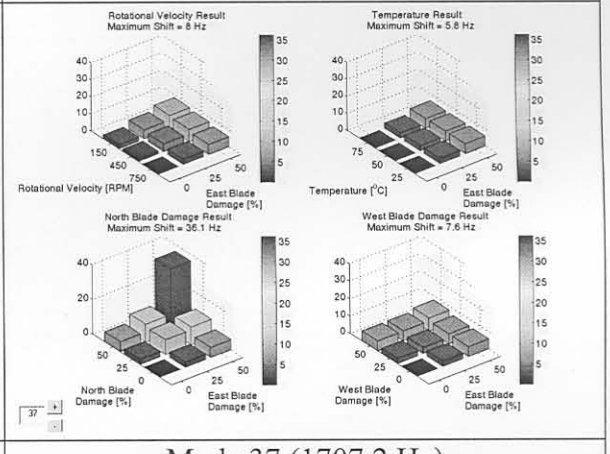

Mode 37 (1707.2 Hz)

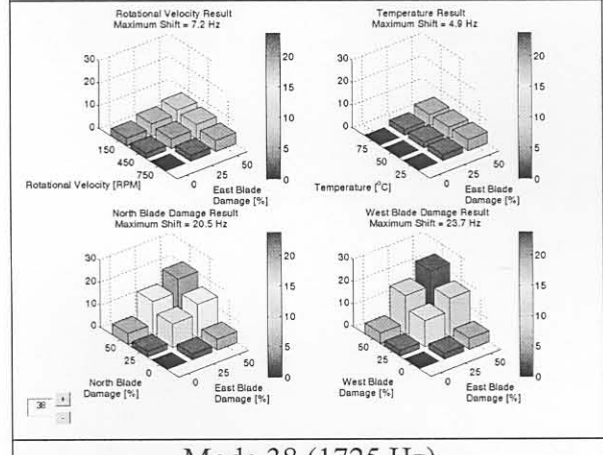

Mode 38 (1725 Hz)

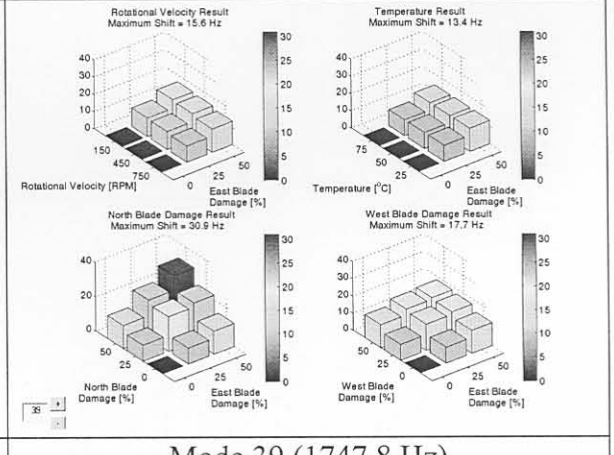

Mode 39 (1747.8 Hz)

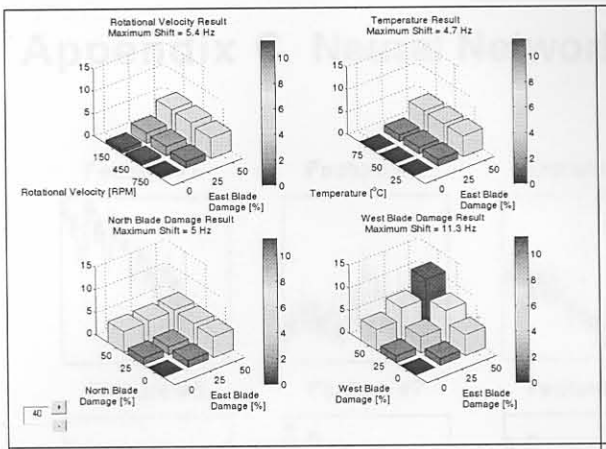

Mode 40 (1792.3 Hz)

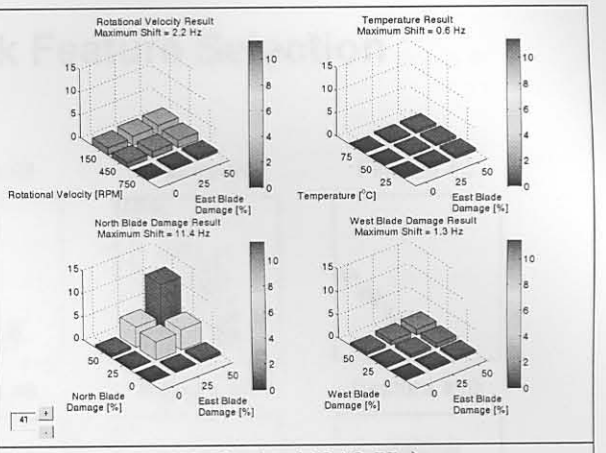

Mode 41 (1810 Hz)

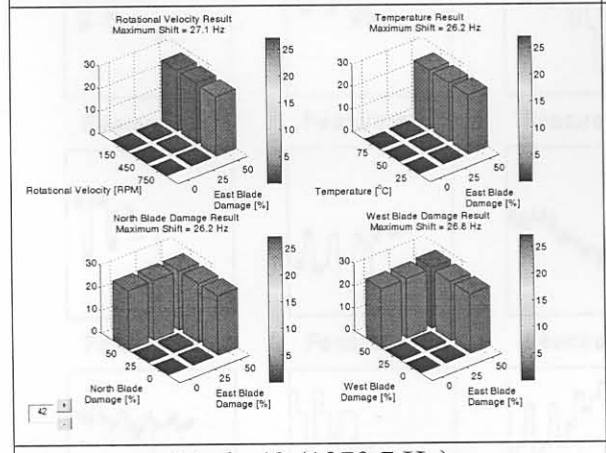

Mode 42 (1970.7 Hz)

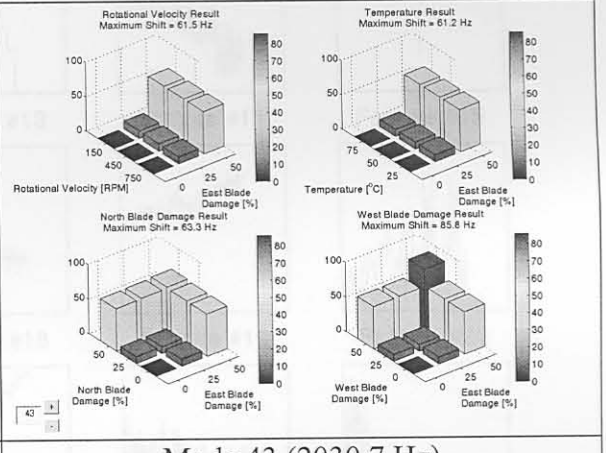

Mode 43 (2030.7 Hz)

Appendix C Neural Network Feature Selection

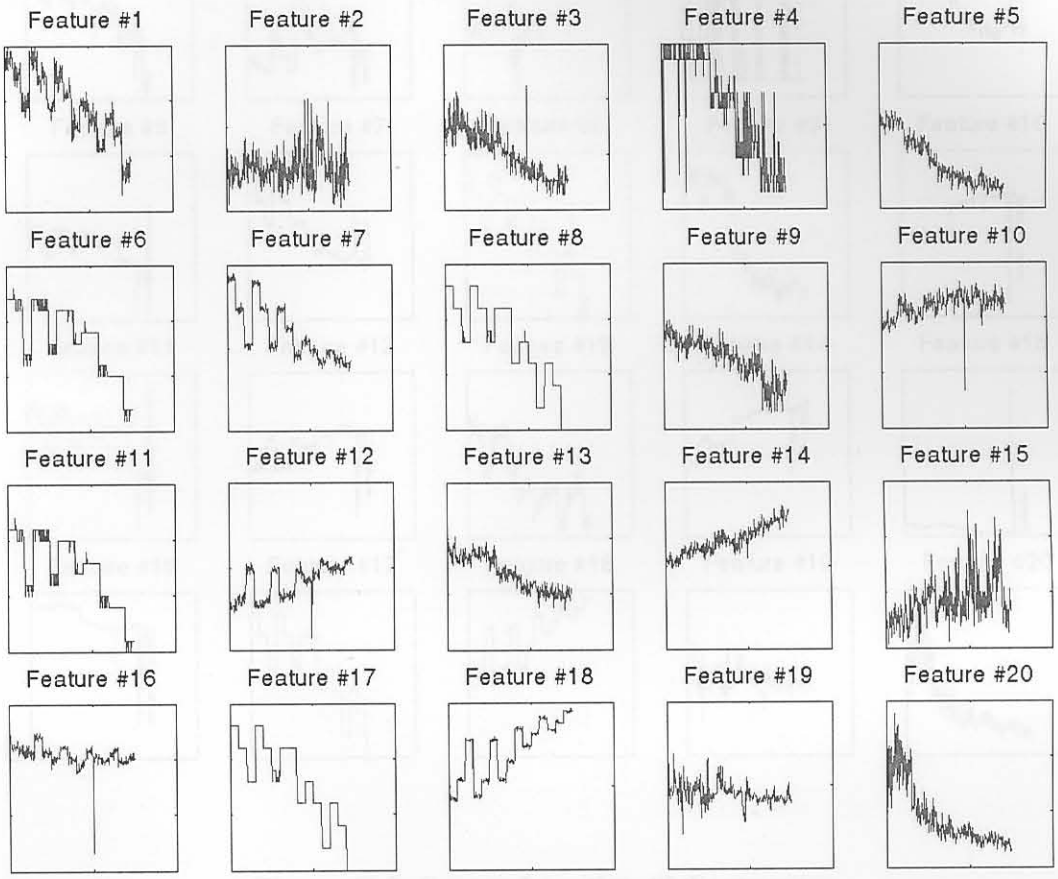

Figure C-1: Sensor Location #1 Feature Selection

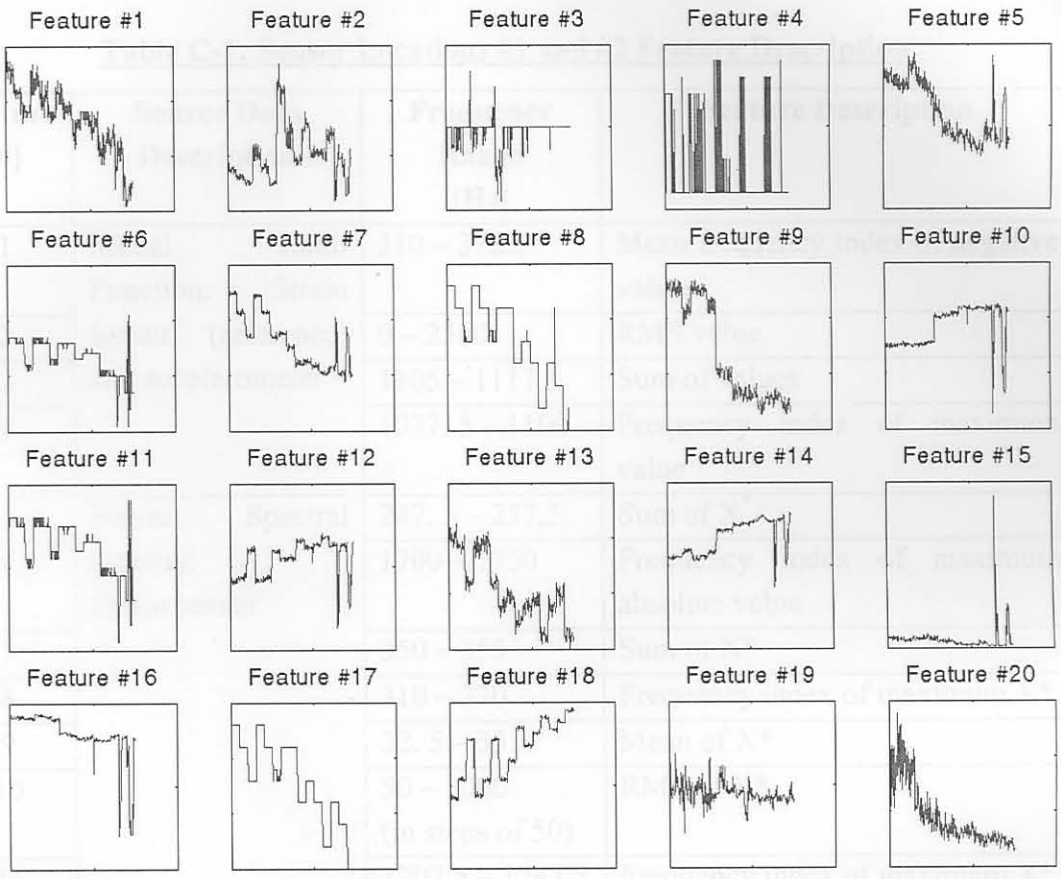

Figure C-2: Sensor Location #2 Features

Table C-1: Sensor Locations #1 and #2 Feature Description

Feature [#]	Source Data Description	Frequency Range [Hz]	Feature Description
1	Modal Ratio Function: Strain sensor (reference) and accelerometer	310 – 372.5	Mean frequency index of negative values
2		0 – 2560	RMS value
3		1105 – 1117.5	Sum of values
4		1077. 5 – 1100	Frequency index of maximum value
5	Power Spectral Density: Strain sensor	247. 5 – 257.5	Sum of X*
6		1700 – 1750	Frequency index of maximum absolute value
7		350 – 355	Sum of X*
8		310 – 370	Frequency index of maximum X*
9		32. 5 – 35	Mean of X*
10		50 – 1000 (in steps of 50)	RMS of X*
11		1702.5 – 1747.5	Frequency index of maximum X*
12		1737. 5 – 1745	Base 10 logarithm of absolute of sum of X*
13		560 – 562.5	Sum of X*
14		1072.5 – 1122.5	Base 10 logarithm of absolute of sum of X*
15		1772. 5 – 1810	RMS of absolute values
16		0 – 2560	Covariance of X*
17	Power Spectral Density: Accelerometer	310 – 370	Frequency index of maximum X*
18		347.5 – 357.5	Base 10 logarithm of absolute of sum of X*
19		0 – 2560	PSDRMS
20		1085 – 1122.5	Sum of absolute values

* X is the base 10 logarithm of the absolute values: $X = \log_{10}(|x|)$

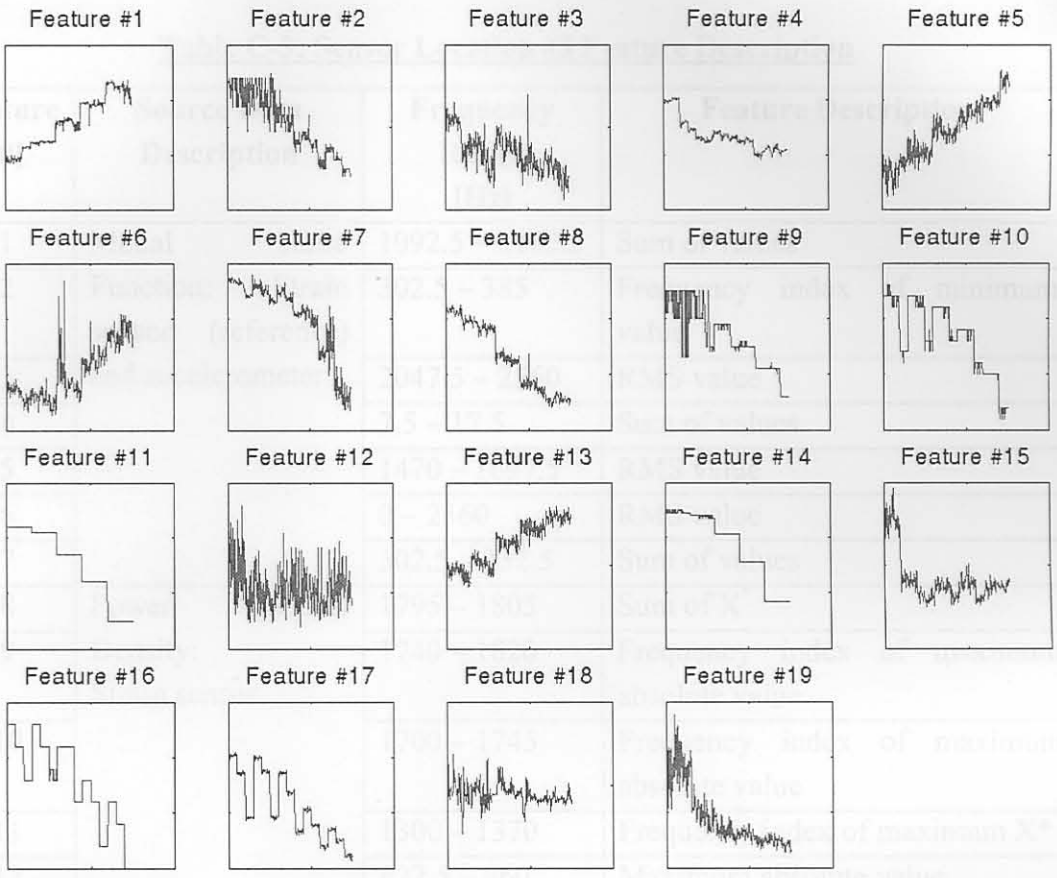

Figure C-3: Sensor Location #3 Feature Selection

Table C-3: Sensor Location #3 Feature Description

Feature [#]	Source Data Description	Frequency Range [Hz]	Feature Description
1	Modal Ratio Function: Strain sensor (reference) and accelerometer	1092.5 – 1102.5	Sum of values
2		302.5 – 385	Frequency index of minimum value
3		2047.5 – 2560	RMS value
4		7.5 – 17.5	Sum of values
5		1470 – 1697.5	RMS value
6		0 – 2560	RMS value
7		302.5 – 332.5	Sum of values
8	Power Spectral Density: Strain sensor	1795 – 1805	Sum of X*
9		1740 – 1820	Frequency index of maximum absolute value
10		1700 – 1745	Frequency index of maximum absolute value
11		1300 – 1370	Frequency index of maximum X*
12		422.5 – 460	Maximum absolute value
13		2172.5 – 2322.5	Natural logarithm of maximum absolute value
14		2172.5 – 2322.5	Frequency index of maximum absolute value
15		0 – 2560	RMS of absolute value
16	Power Spectral Density: Accelerometer	310 – 370	Frequency index of maximum X*
17		347.5 – 357.5	Sum of X*
18		0 – 2560	RMS of X*
19		1085 – 1122.5	Sum of absolute values

* X is the base 10 logarithm of the absolute values: $X = \log_{10}(|x|)$

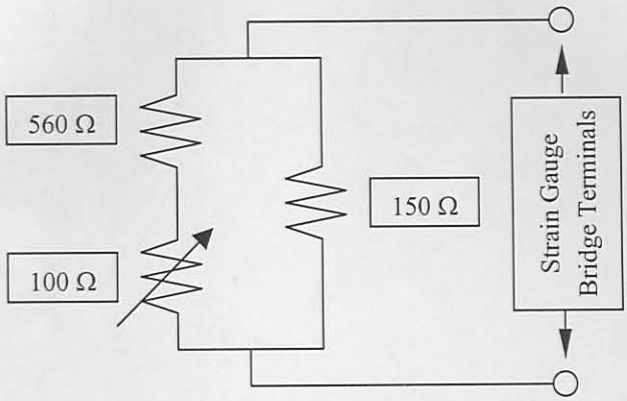

Figure D-2: Half Bridge Completion Circuit

A single 9V PP3 battery performs bridge excitation.
In the second phase of the circuit, the strain gauges signals are amplified with an operational amplifier circuit with a gain of 1000. Power is supplied to the operational amplifier circuit by means of two 9V PP3 batteries. No filtering is performed in the circuit.

The system was tested and validated for static signals.

D.2. System Dynamic Testing

The developed system was tested using a 120 Ω strain gauge rosette installed on the reverse side of on of the FaBCoM TeSt blades as shown in figure D-3. A piezoelectric strain sensor was installed at the same position, but on the front side of the same blade. This was done in order to compare the measurement qualities obtained from the developed system and the piezoelectric system.

Figure D-3: Strain Gauge Rosette Orientation

Several measurements were taken for different conditions to verify the robustness of the developed system in terms of:

- Strain gauge rosette shielding
- Fan rotational velocity
- Motor speed controller noise contribution
- Strain signal amplification before and after the slip ring assembly

Measurements were taken in the form of PSDs from 10 averages with a Siglab signal analyser for a 2 kHz bandwidth with a frequency resolution of 0.625 Hz.

Figure D-4 shows the PSDs for the two systems for rosette shielding, 0 rpm with the motor speed controller switched on and strain signal amplification before sending it through the slip ring assembly. From Figure D-4 it is clear that the developed system has a much higher overall noise floor than the piezoelectric system.

Appendix D Developed Strain Gauge System Testing

The suitability of a developed strain gauge system for on-line blade vibration measurements was tested using conventional strain gauge rosettes. The results are compared with those from a piezoelectric strain gauge system consisting of a piezoelectric strain sensor and signal conditioner.

D.1. Half Bridge Strain Gauge Amplifier

As there were no strain gauge amplifiers with a minimum measurement bandwidth capability of 2000 Hz available for use, it was decided to develop such an amplifier as shown in Figure D-1.

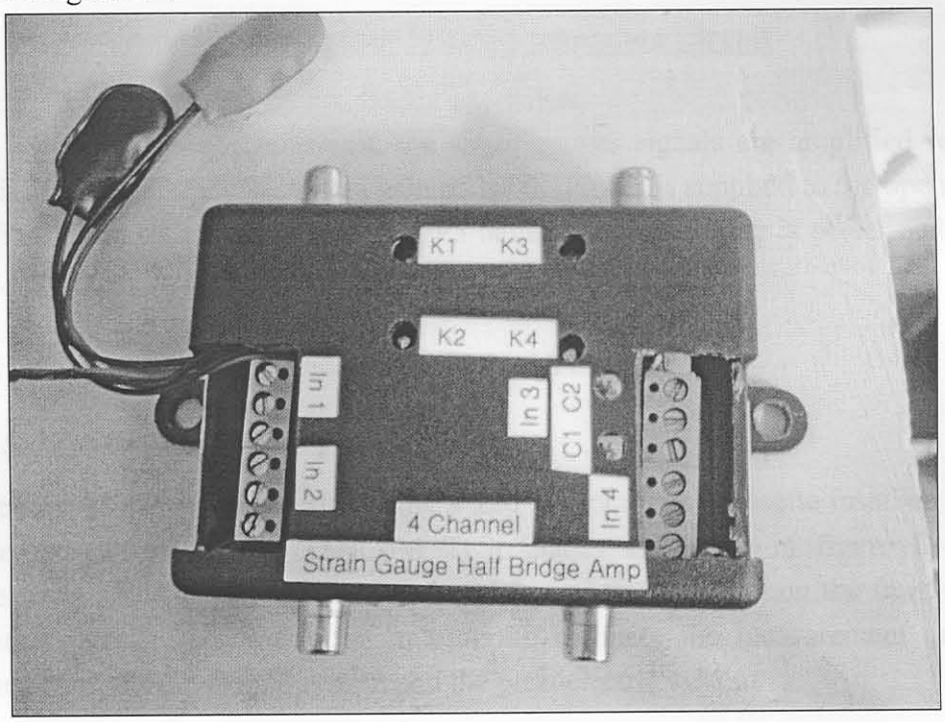

Figure D-1: Four Channel Half Bridge Strain Gauge Amplifier

In the first phase of the circuit, half bridge completion is performed for 120 Ω strain gauges using a dummy resistance circuit as designed by Scheffer [43] as shown in Figure D-2:

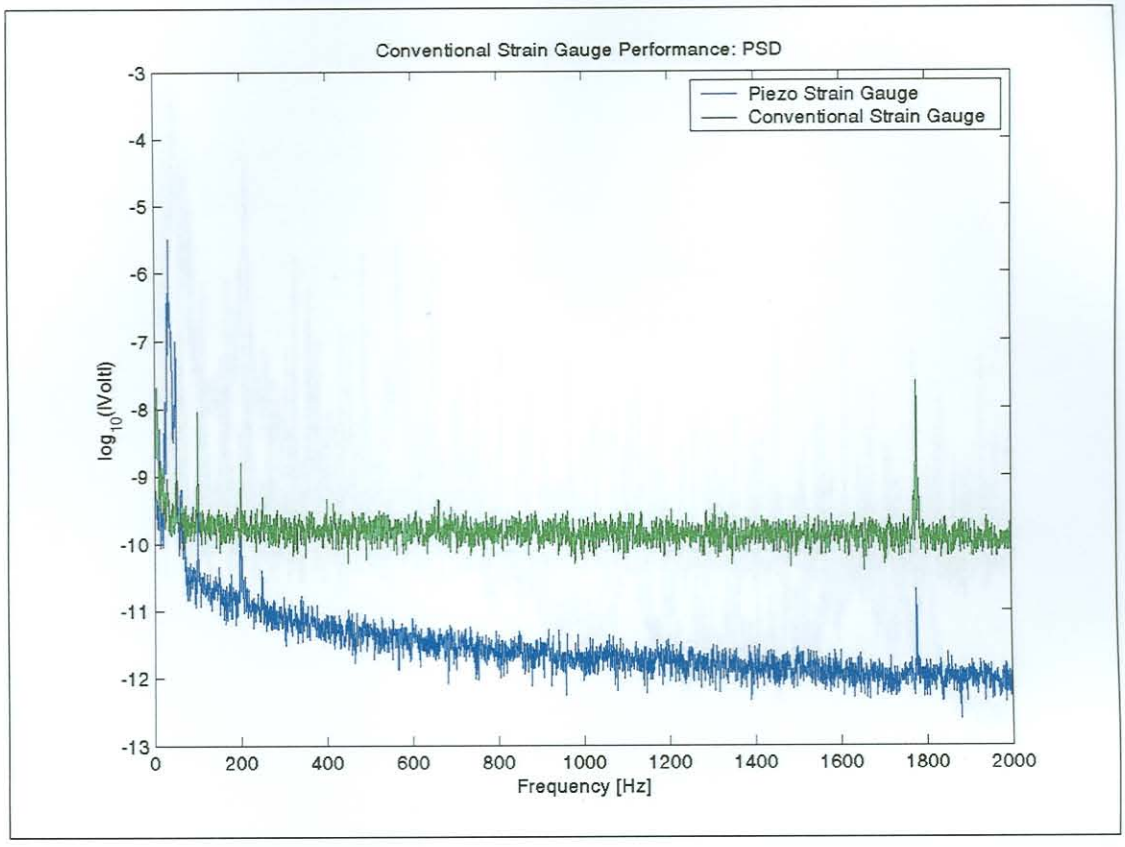

Figure D-4: Strain Gauge PSD Comparison: Ambient Electrical Noise

Figure D-5 shows the two PSDs for the same conditions as for figure D-4, except for a rotational velocity of 750 rpm. As seen in Figure D-5, the piezoelectric strain sensor system gave good results. However, it is also evident that the developed system has an extremely poor signal to noise ratio and that it does not correlate at all with the measurements from the piezoelectric strain sensor system.

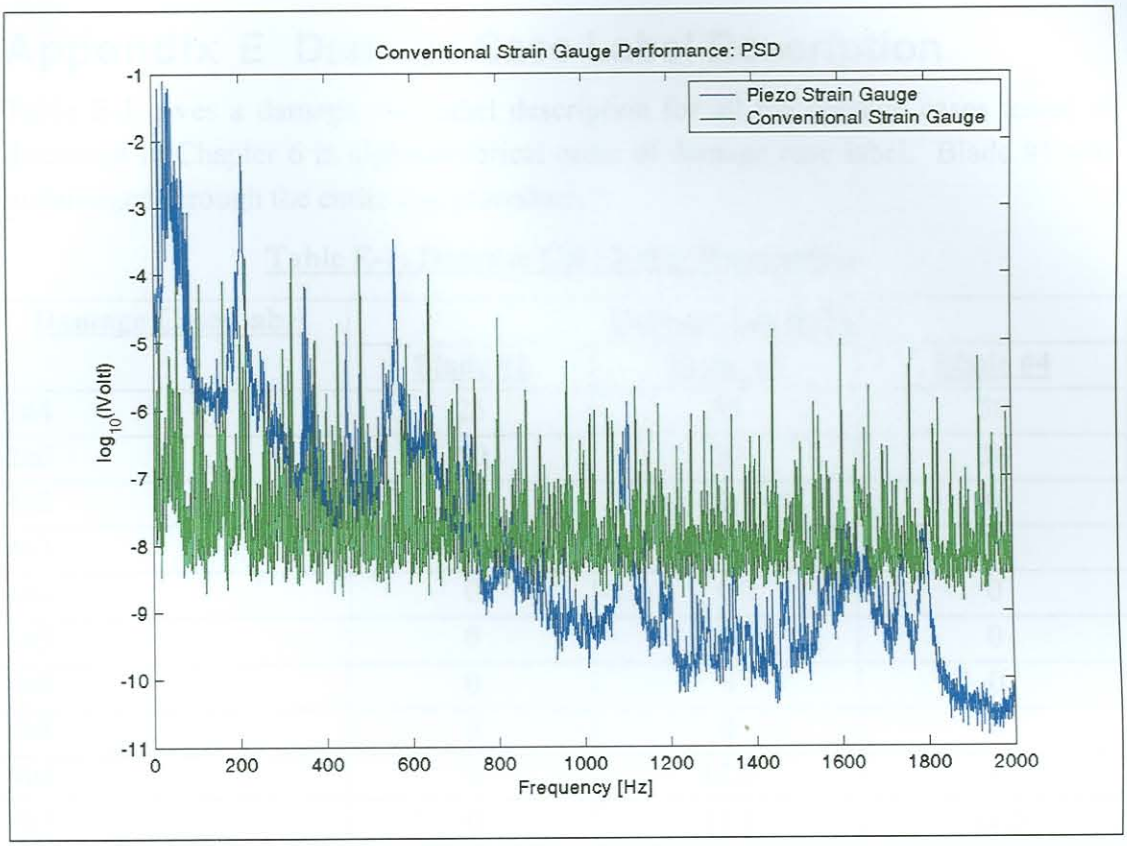

Figure D-5: Strain Gauge PSD Comparison: 750 rpm

D.3. Conclusion

From the tests performed, it is clear that the developed system is not suitable for the application of this dissertation. Possible causes for the poor performance of the system include the lack of signal filtering prior to amplification, the use of an operational amplifier in stead of a differential amplifier as advised by Horowitz and Hill [23] and the lack of system circuitry shielding.

Consequently, it was decided to make use of the piezoelectric strain sensor system.

Appendix E Damage Case Label Description

Table E-1 gives a damage case label description for all the damage cases tested as discussed in Chapter 6 in alphanumerical order of damage case label. Blade #1 was undamaged through the entire test procedure.

Table E-1: Damage Case Label Description

Damage Case Label	Damage Level [%]		
	Blade #2	Blade #3	Blade #4
2a4	25	50	50
2a6	50	50	50
4a2	0	0	0
4a3	0	0	0
4a4	0	0	0
4a5	0	0	0
4a6	0	0	0
4b1	0	0	0
4b2	0	12.5	0
4b3	0	12.5	12.5
4b4	0	12.5	25
4b5	0	12.5	37.5
4b6	0	12.5	50
4c1	0	0	0
4c2	0	25	0
4c3	0	25	12.5
4c4	0	25	25
4c5	0	25	37.5
4c6	0	25	50
4d1	0	0	0
4d2	0	37.5	0
4d3	0	37.5	12.5
4d4	0	37.5	25
4d5	0	37.5	37.5
4d6	0	37.5	50
4e1	0	0	0
4e2	0	50	0
4e3	0	50	12.5
4e4	0	50	25
4e5	0	50	37.5
4e6	0	50	50
4f2	0	50	0

Damage Case Label	Damage Level [%]		
	Blade #2	Blade #3	Blade #4
4f3	0	50	12.5
4f4	0	50	25
4f5	0	50	37.5
4f6	0	50	50